ATMOSPHERIC SCIENCE

Ice nucleation by volcanic ash greatly alters cirrus cloud properties

Lin Lin[1]†, Xiaohong Liu[1]*, Xi Zhao[1]*, Yunpeng Shan[2], Ziming Ke[3], Kai Lyu[1], Kenneth P. Bowman[1]

The formation of ice crystals in the atmosphere strongly affects cloud properties and climate. While volcanic ash (VA) has been shown to nucleate ice crystals efficiently in laboratory settings, its importance for ice formation in the atmosphere remains elusive. Here, we show evidence of cirrus modification by volcanic eruptions through ice nucleation on VA, revealed by abrupt changes in cirrus properties following volcanic eruptions based on satellite measurements. The distinct changes captured are a phenomenal decrease in number, an increase in size of ice crystals in cirrus clouds, and an increase in cirrus occurrences after ash-rich volcanic eruptions. Conversely, no such changes were detected following the ash-poor eruption. We propose a cirrus formation mechanism where VA nucleates ice heterogeneously, suppressing homogeneous freezing and resulting in fewer but larger ice crystals. This suppression of homogeneous freezing by VA is supported by process-level cloud microphysical simulations. Our findings advance the understanding of aerosol–ice cloud interactions and illuminate cirrus geoengineering.

INTRODUCTION

The interaction between aerosols and clouds remains one of the largest sources of uncertainty in understanding Earth's climate and projecting its future changes. Cirrus clouds (*1*), the high-altitude clouds composed entirely of ice crystals and ubiquitous in the upper troposphere and lower stratosphere, tend to exert a net warming effect on the planet (*2*). Ice nucleating particles (INPs), rare yet crucial aerosols, play a critical role in initiating the formation of ice crystals and thus can influence the radiative effect of cirrus clouds by changing their microphysical properties (*3*). Early studies have suggested that volcanoes are an important source of atmospheric INPs (*4*, *5*). These INPs, which consist of a mixture of rock, mineral, and glass particles < 2 mm in diameter, are primarily volcanic ash (VA). Recent laboratory studies have confirmed that VA particles collected from various volcanoes worldwide can nucleate ice across a wide range of atmospheric conditions (*6*–*9*), including a cirrus cloud formation pathway through deposition-mode ice nucleation (*10*, *11*). Therefore, VA particles may affect cirrus cloud properties and modulate the Earth-atmosphere energy balance. For instance, ground-based and satellite atmospheric observations suggested that the Kasatochi eruption likely led to cirrus cloud seeding in the upper troposphere by mixing in the VA and large sulfate-based solution droplets from the lower stratosphere via a tropopause fold (*12*). Although it has been discussed in the community that volcanic eruptions could lead to cirrus modification, hard evidence is difficult to find. Observational evidence of the indirect climate impacts of VA (*13*, *14*) is scarce due to the complexity of atmospheric processes and a general lack of large-scale aerosol and cloud measurements, limiting our understanding of the radiatively important clouds and their feedback to climate change.

Ice crystals in cirrus can form through two competing nucleation mechanisms—homogeneous and heterogeneous ice nucleation—with the dominant mechanism largely determining cirrus microphysics properties, such as ice crystal number concentration and size (*15*–*17*). Homogeneous nucleation takes place on abundant solution aerosols at temperatures below −38°C and relative humidities with respect to ice (RH_{ice}) above 140 to 160%. This process leads to the formation of dense clouds composed of small ice crystals characterized by high number concentrations of ~100 to 10,000 liter^{-1} at updraft velocities in the range of 10 to 100 cm s^{-1} (*18*). INPs (e.g., VA and mineral dust), which make up only 1 in 10^3 to 10^6 ambient aerosol particles, have surface properties that lower the energy barrier for ice nucleation so that they facilitate ice nucleation heterogeneously at lower RH_{ice} than required for homogeneous nucleation. Consequently, INP-initiated cirrus usually contains fewer ice crystals, with number concentrations of ~1 to 100 liter^{-1}, due to the rarity of INPs (*19*). The presence of INPs can delay or entirely suppress the homogeneous nucleation because heterogeneous nucleation precedes and preferentially consumes water vapor to the extent that the high RH_{ice} required for the onset of homogeneous freezing is not reached (*15*–*22*); while the actual impact of heterogeneous nucleation depends on updraft velocity, the number and type of INPs. This homogeneous-heterogeneous competition leads to an overall reduction in ice crystal number—a phenomenon termed as the "negative-Twomey effect" (*22*), as opposed to the conventional Twomey effect (*23*) which describes an increase of cloud droplet number concentrations with increasing aerosol abundances in warm clouds.

On the basis of the dissimilar behaviors of cirrus of different origins, we contrast the microphysical properties of cirrus clouds with and without VA perturbations in the lowermost stratosphere (LMS) at midlatitudes. This comparison helps to infer the likelihood of VA's negative-Twomey effect on cirrus. The choice of midlatitude LMS as a natural testbed (Materials and Methods) lies in the increasing susceptibility of in situ optically thin cirrus clouds to VA perturbations. Under unperturbed conditions without aerosols from volcanic eruptions and wildfires, the LMS is presumed to be a pristine environment with abundant sulfate aerosols (*24*–*28*). This suggests that the predominant nucleation mechanism is homogeneous nucleation on sulfate aerosols (section S1) driven by the frequently observed updraft speeds of ~10 to 20 cm s^{-1} in mesoscale gravity waves (*29*–*32*). VA from explosive volcanic eruptions present in the LMS could shift the dominant nucleation mechanism to heterogeneous nucleation. Previous studies (*16*, *18*, *32*) show that heterogeneous nucleation

[1]Department of Atmospheric Sciences, Texas A&M University, College Station, TX, USA. [2]Argonne National Laboratory, Lemont, IL, USA. [3]Lawrence Livermore National Laboratory, Livermore, CA, USA.
*Corresponding author. Email: xiaohong.liu@tamu.edu (X.L.); zhaoxinuist@126.com (X.Z.)
†Present address: Lawrence Livermore National Laboratory, Livermore, CA, USA.

begins to inhibit homogeneous nucleation at low concentrations of INPs (<10 liter^{-1}). We thus hypothesize that even a moderate amount of VA with potent ice nucleating ability would suffice to restrain the homogeneous freezing and produce transformed cirrus clouds characterized by fewer ice crystals. These drastic shifts in cirrus properties can reveal VA-cirrus causality if meteorological covariability is excluded. We test our hypothesis by using recent explosive volcanic eruptions at midlatitudes, which injected VA and gases into the LMS (Materials and Methods).

Recent advancements in aerosol extinction, aerosol subtyping (*33*–*36*), and cirrus ice retrievals (*37*) using spaceborne radar-lidar with vertical profiling capabilities enable the impacts of VA on cirrus properties to be explicitly studied on a large spatiotemporal scale. In this work, by integrating these new satellite capabilities, we examine changes in cirrus microphysical properties following three extratropical volcanic eruptions. Our results show substantially fewer but larger ice crystals in post-eruption midlatitude cirrus clouds during periods of frequent VA occurrences, indicative of VA's negative-Twomey effect on cirrus. This suppression of homogeneous nucleation by VA is further corroborated by detailed cloud microphysical simulations of ice nucleation. This study reveals an important role of VA as INPs in the atmosphere and serves a better understanding of impacts of volcanic eruptions on cirrus cloud characteristics with broader climate implications.

RESULTS

Distinguishing ash-rich and ash-poor eruptions based on aerosol characteristics

The three volcanic eruptions studied are the 2008 Kasatochi, 2009 Sarychev, and 2015 Calbuco (Materials and Methods and table S1). At their respective hemispheric midlatitudes in the LMS, each eruption radically elevated the aerosol extinction, a proxy for aerosol loading, for several months (Fig. 1 and fig. S1). Therefore, months of aerosol enhancement during and after each eruption are identified as volcanically perturbed periods: August to December 2008 for Kasatochi, June to December 2009 for Sarychev, and April to December 2015 for Calbuco. For comparison, we define unperturbed periods as mid-2012 to 2016 in the Northern Hemisphere (Fig. 1A) and 2007 to 2014 in the Southern Hemisphere (Fig. 1B), during which aerosol extinction levels were reduced.

We use the CALIPSO (Cloud-Aerosol Lidar and Infrared Pathfinder Satellite Observation) vertical feature classification flags (Materials and Methods) to identify aerosol types. Figure 2 shows the comparison of occurrence frequencies of VA and sulfate aerosol between the volcanically perturbed and unperturbed periods. Because of the direct injection of VA, more frequent VA occurrences are observed immediately after the eruptions of Kasatochi and Sarychev (at month 0) compared to the unperturbed periods (Fig. 2A). The frequent VA occurrences are supported by remote-sensing and in situ measurements, which show that fine ash particles can remain in the LMS for months to a year after a major eruption (*38*–*42*). In contrast, the occurrence of VA after the 2015 Calbuco eruption is comparable to the unperturbed level. We hypothesize that these frequent VA occurrences indicate the presence of more VA particles. We categorize the Kasatochi and Sarychev eruptions as ash rich and Calbuco eruption as ash poor.

In the ash-rich scenario, the occurrence frequency of sulfate aerosol evolves in phase with that of VA (Fig. 2B). Zhu *et al.* (*43*) demonstrated that the presence of VA effectively induces the production of sulfate through heterogeneous reactions on VA surfaces and meanwhile reduces the overall burden and lifetime of sulfur species due to

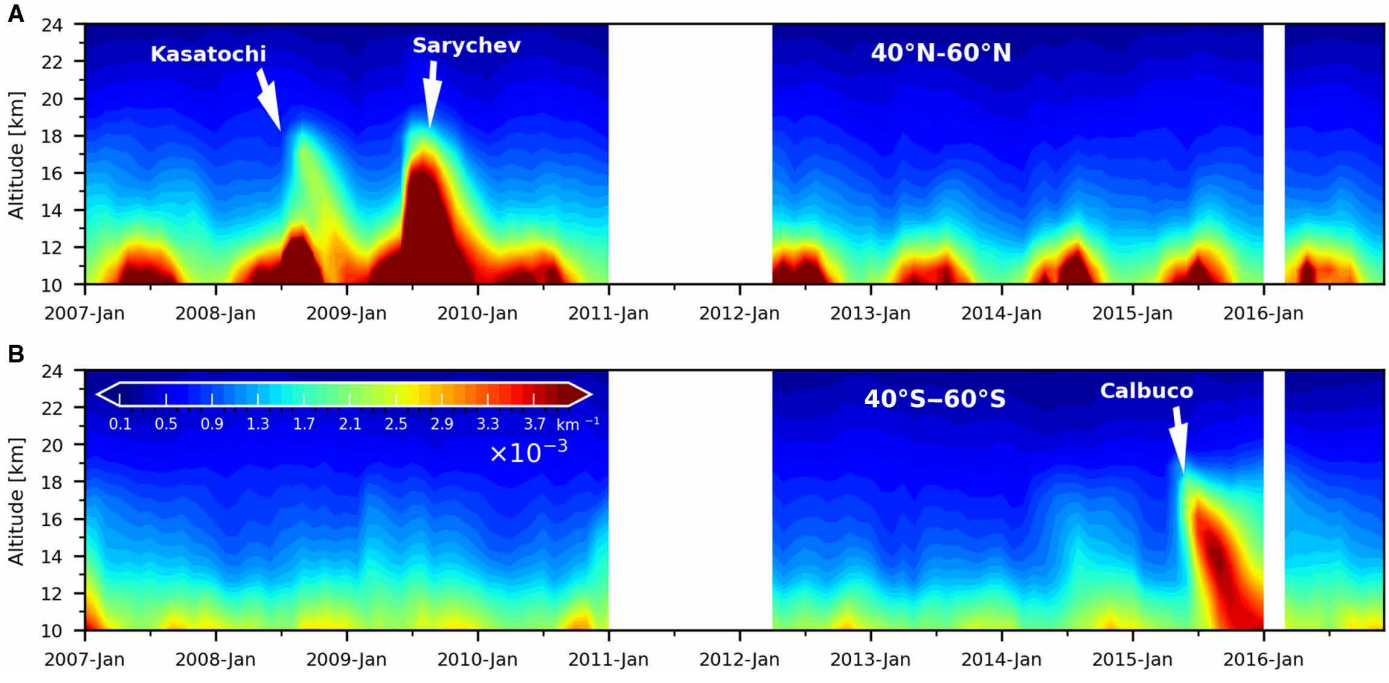

Fig. 1. Stratospheric aerosol perturbations. Retrieved 532-nm aerosol extinction coefficient (km^{-1}) from the CALIPSO L3 stratospheric aerosol profile product over (**A**) Northern Hemisphere midlatitudes (zonal average over 40°N to 60°N) and (**B**) Southern Hemisphere midlatitudes (zonal average over 40°S to 60°S). Blank areas indicate periods when cloud or aerosol data are missing (January 2011–April 2012; February 2016). Volcanically perturbed periods: August–December 2008, June–December 2009, and April–December 2015. Unperturbed periods: Mid-2012 to 2016 in the Northern Hemisphere and 2007 to 2014 in the Southern Hemisphere.

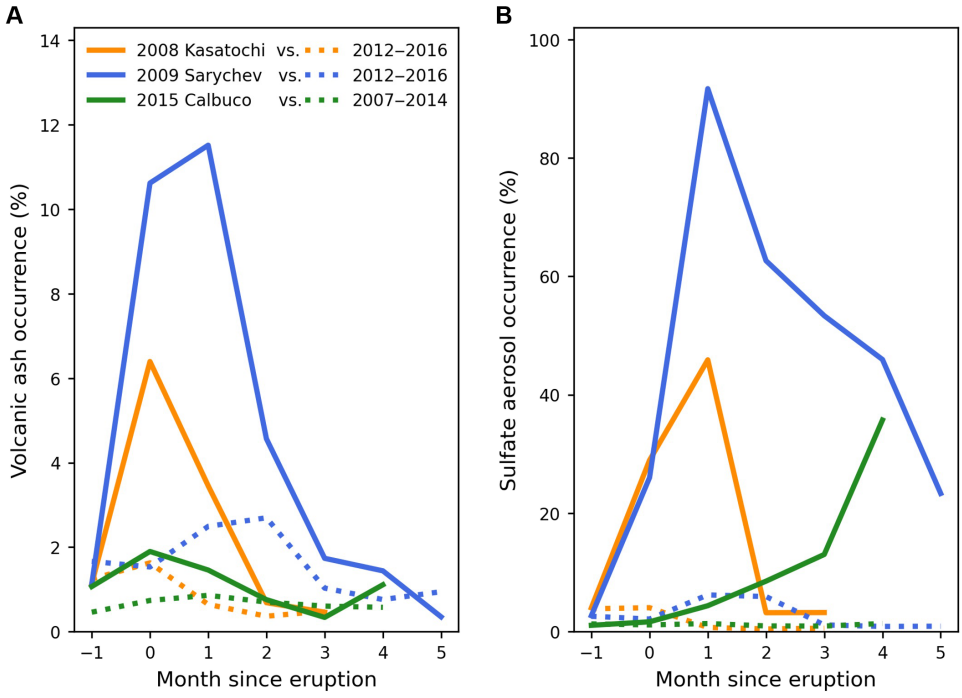

Fig. 2. High occurrence frequency of VA detections during and after the Kasatochi and Sarychev eruptions. Temporal evolution of frequency of occurrence of (**A**) VA and (**B**) sulfate aerosol in the lower stratosphere relative to the month when the 2008 Kasatochi, 2009 Sarychev, and 2015 Calbuco volcanoes erupted (i.e., month 0 is August, July, and April, respectively), as compared to the respective unperturbed periods (i.e., July to December 2008 versus 2012–2016; May to December 2009 versus 2012–2016; March to December 2015 versus 2007–2014, respectively). Vertical feature classification data over the latitudinal zonal bands of 50°N to 60°N, 40°N to 60°N, and 40°S to 60°S are analyzed for eruptions of Kasatochi, Sarychev, and Calbuco, respectively. The Kasatochi volcano erupted on 7 to 8 August 2008. The Sarychev volcano erupted on 12 June 2009. The Calbuco volcano erupted on 22 April 2015.

uptake on falling VA. Signatures of in-phase versus out-of-phase of sulfate occurrences further confirm the presence of VA in the ash-rich scenario and its absence in the ash-poor scenario. In addition, a lack of hydroxyl radicals during the austral winter delayed the production of sulfate aerosols after the Calbuco eruption in late April 2015.

Abrupt changes in cirrus microphysics following ash-rich eruptions

To investigate the impacts of VA on cirrus, we contrast the number concentration (N_i) and effective radius (r_{eff}) of ice crystals in LMS cirrus clouds between the volcanically perturbed and unperturbed periods for each volcanic event. This comparison is conducted over the same geographical domain and time frame as used in the aerosol subtype analysis, ensuring consistency in our aerosol and cloud analyses. By examining changes in N_i and r_{eff}, we aim to elucidate the mechanism through which VA influences cirrus cloud microphysics.

Compared to values observed during the unperturbed periods, both the mean and median N_i exhibit a marked decrease by ~80% within 1 to 2 months following the ash-rich eruptions of Kasatochi and Sarychev (Fig. 3, A and B). This decrease in N_i, which persists for several months, is statistically significant in which the changes fall below the 25th percentile range of long-term statistics. After reaching a local minimum, N_i gradually returns to unperturbed levels. In addition, we observe a clear shift in the N_i probability distribution function (PDF) toward smaller values during the perturbed periods (Fig. 3, D and E). A full analysis of the month-to-month N_i PDF shows a deviation from climatology as soon as an eruption occurs (figs. S2 and S3). Meanwhile, the r_{eff} PDF shifts toward larger values, with a ~12% increase in peak values from 17 to 19 μm in the aftermath of the ash-rich eruptions (Fig. 3, G and H). Similarly, a full analysis of the month-to-month r_{eff} PDF (figs. S5 and S6) shows a deviation from climatology immediately after an eruption occurs.

Ice water contents (IWCs), a parameter not directly subject to the perturbation of ice nucleation like N_i, also show a simultaneous decrease (figs. S8 and S9, A and C), possibly because of enhanced gravitational settling from increased ice crystal sizes. In addition, we note that the observed changes in cirrus ice microphysics are consistent, albeit, to a lesser extent, when extending our analysis to the upper troposphere (figs. S8 to S10). A detailed discussion of the observed changes in cirrus cloud microphysics is provided in section S2.

The magnitude and timing of the observed decreases in N_i cannot be explained by seasonal variability or meteorological covariability (i.e., temperature, humidity, and vertical velocity; see figs. S11 to S20 and Materials and Methods). For this study which covers large-scale geographical areas with volcanic perturbations lasting for months, we confirm that cloudy scenes containing fewer ice crystal tend to occur more frequently at cirrus-relevant temperatures when binned into smaller ranges (fig. S21 and section S3). The decrease in N_i is independent of temperature.

Furthermore, temporal evolutions of N_i and stratospheric aerosol extinction show remarkably good inverse relations for ash-rich eruptions (fig. S22). The association between N_i and aerosol extinction trends can be further examined by ignoring the time dimension and analyzing N_i change as a function of the aerosol extinction change. This reveals a strong correlation (with correlation coefficient of 0.68 to 0.85) between N_i decrease and aerosol enhancement for

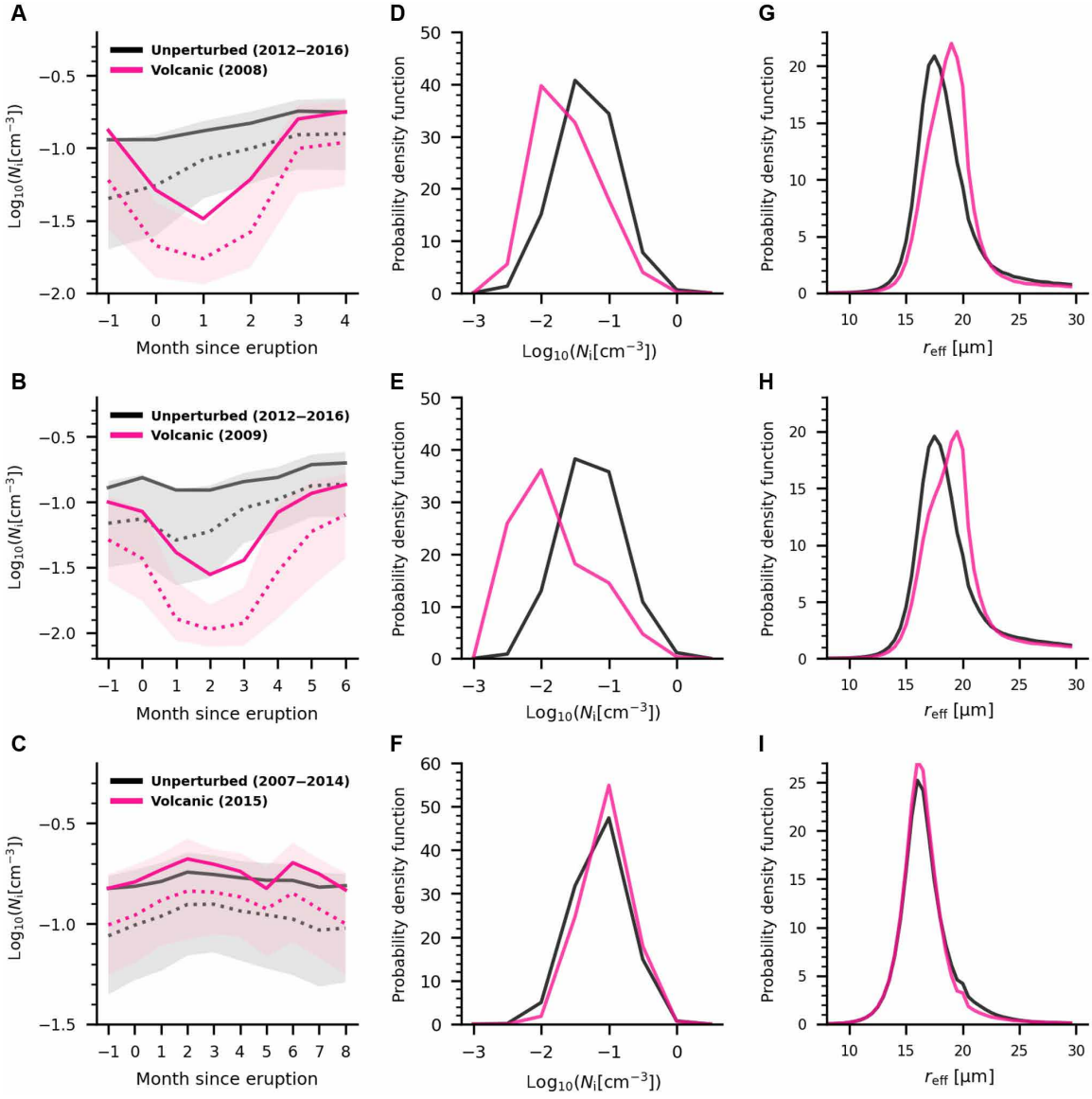

Fig. 3. Abrupt changes in cirrus ice crystal number concentration and effective radius are observed after ash-rich eruptions. The temporal evolution of the monthly mean (solid line) and median (dotted line) ice crystal number concentration (N_i) during volcanically perturbed periods (pink line) is shown relative to the month of eruption of the (**A**) 2008 Kasatochi, (**B**) 2009 Sarychev, and (**C**) 2015 Calbuco volcanoes (i.e., month 0 is August, July, and April, respectively), compared to the respective unperturbed periods (black line). Shaded areas denote the 25th and 75th percentiles. PDFs for N_i (**D** to **F**) and effective radius r_{eff} (**G** to **I**) are presented for the volcanically perturbed versus unperturbed periods. Observations over 50°N to 60°N in 2008 versus 2012–2016 for Kasatochi [(A), (D), and (G)]; 40°N to 60°N in 2009 versus 2012–2016 for Sarychev [(B), (E), and (H)]; 40°S to 60°S in 2015 versus 2007–2014 for Calbuco [(C), (F), and (I)]. The Kasatochi volcano erupted on 7 to 8 August 2008, the Sarychev volcano erupted on 12 June 2009, and the Calbuco volcano erupted on 22 April 2015. See tables S2 to S4 for details of observational data.

ash-rich eruptions (fig. S23), indicating a perturbation of cirrus microphysical properties by volcanic aerosols. The sign of observed N_i variations contradicts the general expectation that N_i would increase due to homogeneous freezing of elevated sulfate aerosol loads (*44*) after a major eruption. Instead, concurrent and opposing changes in N_i and r_{eff} after ash-rich eruptions suggest a transition from cirrus formation dominated by homogeneous to heterogeneous nucleation, consistent with the hypothesis of a negative-Twomey effect exerted by VA. A similar negative-Twomey effect is documented for mineral dust and anthropogenic aerosol (*45*), corroborating the ice nucleating activities of VA. Moreover, cirrus clouds sampled during ash-rich periods tend to occur more frequently (fig. S24). VA promotes ice formation at lower RH_{ice} than is possible with only homogeneous nucleation, thus cirrus forms favorably when VA is present. VA perturbations increase the occurrence frequency of cirrus clouds. Multiple lines of evidence suggest that VA particles in the LMS serve as efficient INPs, initiating heterogeneous ice nucleation and suppressing homogeneous nucleation from producing abundant ice crystals, although homogeneous nucleation may not be completely switched off depending on the cloud updraft conditions.

In stark contrast, we observe no similar changes in N_i, r_{eff}, and IWC, nor an inverse correlation between N_i and aerosol extinction

trends following the ash-poor 2015 Calbuco eruption [Fig. 3 (C, F, and I) and figs. S4, S7, S8, S10 (E and F), S22C, and S23C]. Intuitively, we would expect a greater influence on cirrus cloud properties with VA addition in the Southern Hemisphere, given its more pristine background with minimal INP influence, as opposed to the Northern Hemisphere with ample sources of mineral dust and busier aviation traffic (*46*, *47*). However, we observe only a marginal increase in N_i (~26% on average), nearly unchanged r_{eff} (Fig. 3) and no obvious correlations between N_i and aerosol extinction trends (figs. S22C and S23C). Microphysical studies of stratospheric sulfate geoengineering (*44*) show that continuous SO_2 injection into the stratosphere leads to more abundant ice crystals. From this, it is inferred that sulfate aerosols produced from eruptions may analogously lead to the formation of more ice crystals, although the susceptibility of homogeneously nucleated N_i to the number concentration of solution droplets is relatively weak (*48*–*50*). The contrasting behavior of cirrus clouds in response to an ash-poor eruption lends credence to the hypothesis of a negative-Twomey effect on cirrus caused by VA, whereby the presence of VA suppresses homogeneous nucleation, leading to fewer but larger ice crystals.

Microphysical simulations on homogeneous freezing suppression by ashes

We use a detailed microphysical ice nucleation model (Materials and Methods) to investigate how midlatitude LMS cirrus clouds respond to varying levels of sulfate and VA abundance. Our model represents the competing processes of homogeneous and heterogeneous ice nucleation, enabling simulations of ice formation under both ash-poor and ash-rich conditions. By varying the concentrations of sulfate aerosols and VA particles, our simulations provide insights into how different nucleation mechanisms influence cirrus cloud microphysics, especially N_i. This modeling approach allows us to assess the impacts of VA on cirrus cloud properties under different meteorological and aerosol conditions, particularly the negative-Twomey effect, and to distinguish the aerosol effect between the ash-rich versus ash-poor volcanic eruptions.

Our simulations show that under the ash-poor condition, even substantial additions of sulfate aerosols of volcanic origin to the background LMS result in only minor increases in N_i (Fig. 4A) (*48*–*50*), confirming that sulfate aerosols alone have limited impact on N_i. This outcome aligns with the observed N_i changes following the 2015 Calbuco eruption, where the primary nucleation mechanism was assumed to be homogeneous freezing of sulfate. This supports the conclusion that a lack of VA causes no outstanding changes in cirrus properties, as observed in the ash-poor scenario.

Heterogeneous nucleation of VA expedites the onset of ice formation and precedes homogeneous nucleation. Under typical vertical velocities of 10 to 20 cm s^{-1} in the LMS (with results shown for 15 cm s^{-1}), homogeneous nucleation remains the dominant mechanism for producing the total N_i when VA concentrations are ≤1 $liter^{-1}$ competing for water vapor, resembling conditions in the ash-poor scenario (as depicted in the leftmost portion of Fig. 4B compared to Fig. 4A). However, as VA concentrations increase to approximately 10 $liter^{-1}$, N_i plummets (Fig. 4B). The overall reduction in N_i is attributed to heterogeneous nucleation now suppressing homogeneous nucleation and becoming the primary process for ice crystal formation although limited by VA scarcity. Earlier microphysical simulations (*51*) also found a notable reduction of ice numbers when ice nucleated heterogeneously on volcanic silicate particles. The range of

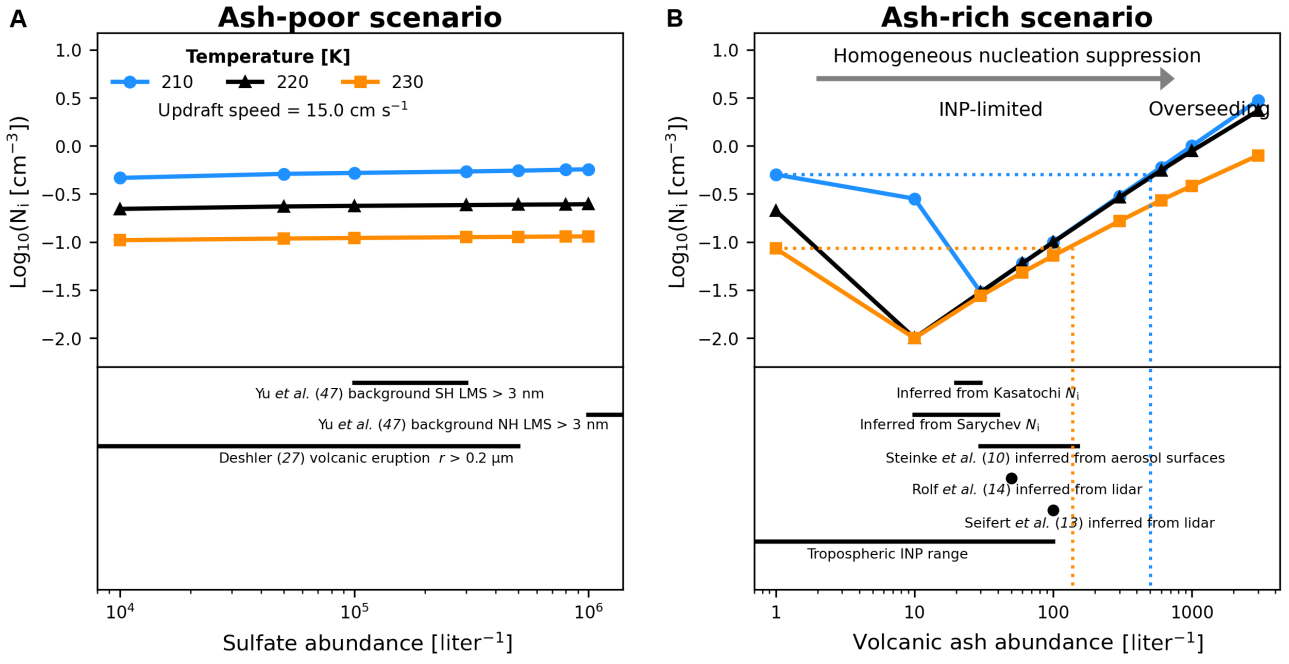

Fig. 4. Simulated ice crystal number concentration for ash-poor and ash-rich scenarios. (**A**) Homogeneous nucleation-induced N_i is shown as a function of sulfate aerosol abundance over LMS cirrus–relevant temperature ranges. (**B**) Homogeneous and heterogeneous nucleation compete as a function of VA particle abundance. Bottom displays typical ranges of sulfate aerosol abundance in the LMS [Deshler (*27*); Yu *et al.* (*47*)] and VA particle abundance in the LMS and the upper troposphere [Steinke *et al.* (*10*); Seifert *et al.* (*13*); Rolf *et al.* (*14*)] derived from laboratory, remote-sensing, and modeling studies. The VA particle abundances inferred from the minimum N_i in Fig. 3A correspond to Kasatochi, while those from Fig. 3B correspond to Sarychev. Typical ranges of tropospheric INPs are also included. Ranges of VA particle and tropospheric INPs abundances fall within the INP-limited regime. NH, Northern Hemisphere; SH, Southern Hemisphere.

VA abundance where the negative-Twomey effect is triggered is termed as the INP-limited regime.

Furthermore, after reaching a local minimum, N_i would increase again if VA concentrations continued to rise until a critical threshold VA concentration where heterogeneously induced N_i equals to that from homogeneous nucleation. Surpassing this threshold results in the overseeding regime. VA has been documented to act as INPs overseeding cirrus clouds (*14*, *52*), leading to larger N_i and smaller r_{eff} relative to the dynamically similar unperturbed clouds. However, this overseeded cirrus, captured by lidar at a point near emission sources, may only occur briefly with momentarily high concentrations of VA. Over a large spatiotemporal scale, as in this study, it is reasonable to expect low VA concentrations in the LMS due to dispersion and dilution after injection.

Hypothetically, if the observed N_i minimum in the ash-rich scenario (Fig. 3, A and B) is indeed caused by heterogeneous nucleation of VA, then the inferred VA concentration from that N_i minimum is about 13 to 20 liter^{-1}. This VA concentration aligns well with the lowest N_i values in the INP-limited regime (Fig. 4B). VA INPs with freezing thresholds slightly above ice saturation are capable of introducing strong changes of cloud properties, even at low concentrations. Optically thin and subvisible cirrus that often occur in the LMS are found to be particularly susceptible to INP perturbations (*18*). Under the typical thermodynamic and dynamic conditions of the LMS assumed in the model, the VA concentration that starts to suppress homogeneous nucleation is comparable to that of other INPs on the order of 10 liter^{-1}. This is consistent with concentrations typical of northern midlatitude background conditions (<10 to 30 liter^{-1}), which can greatly modify cirrus properties. The exact value, however, depends on factors such as cloud formation temperature, updraft velocity, and freezing relative humidity.

According to the ice nucleation theory, after disentangling the influence of meteorological factors, there is no other route except heterogeneous nucleation on VA to account for the counterintuitive phenomenon where an increase in aerosol loads coincides with a decrease in N_i. By isolating the effects of VA from other variables, we demonstrate that VA particles effectively suppress the homogeneous nucleation, leading to fewer ice crystals—a phenomenon known as the negative-Twomey effect. Our carefully designed natural experiment provides potential evidence of the ash-cirrus causality. This finding highlights the unique role of VA in altering cirrus cloud microphysics through heterogeneous ice nucleation.

DISCUSSION

Volcanic sulfate is known to exert an important influence on climate through both direct and indirect radiative forcing mechanisms (*53*–*55*). However, the role of VA in cirrus cloud formation remains less understood. The three recent volcanic eruptions present a unique opportunity to investigate hemispheric-scale ash-cirrus cloud interactions. Synergistic satellite retrievals and microphysics simulations support the hypothesis that the inverse relationship between increases in VA aerosols and abrupt decreases (increases) in N_i (r_{eff}) is caused by heterogeneous ice nucleation on VA, schematically shown in Fig. 5. Lower stratospheric water vapor enhancement following the three eruptions is found to last for a few days downwind of the injection locations (*56*). As a result, water vapor increases in the volcanic plume have a minimal effect on the total water vapor available for cirrus formation and crystal growth.

The recurrent injection of substantial amounts of VA particles into cirrus-forming regions, where they can persist for extended periods, underscores VA as an important source of ice-cloud INPs. The ice nucleating activities of VA, which complement those of other well-defined INPs like mineral dust, contribute to additional cloud radiative effects. This highlights the importance of considering VA in climate models to better understand and predict the climatic impacts of volcanic eruptions.

To date, studies of the impact of volcanic aerosol on cirrus clouds have primarily used climate models that exclusively incorporate sulfate aerosols (*57*, *58*). The omission of VA and its ice nucleation activity limits our ability to explore other potential ice nucleation pathways and their competing effects on the formation, lifetime, and radiative properties of cirrus clouds. Nowadays, a growing body of research has begun to incorporate VA into models, highlighting its critical role in improving simulations of stratospheric chemistry and dynamics (*43*, *59*). It is imperative to include VA into climate models and link it to cloud microphysical processes for advancing our understanding of their impact on cirrus cloud microphysics and Earth's energy budget. Nevertheless, major challenges exist. Accurate modeling of VA's indirect climate effect requires information on emission quantity, injection height, and aerosol microphysical properties and processes, such as density and size distribution, dry and wet deposition, mixing of VA with sulfate, and parameterizations of VA's ice nucleating ability and nucleation mode. In addition, the subgrid scale updraft velocity induced by mesoscale gravity wave dynamics is a key parameter for determining the underlying nucleation mechanism and quantifying ice crystal numbers (*60*). Unfortunately, such detailed information is now lacking due to insufficient observations for specific volcanic eruptions and for each cirrus instance. To narrow the knowledge gap, close collaborations between atmospheric scientists and volcanologists are crucial. Such coordinated efforts can enhance our ability to gather the necessary observational data and to refine the current models, ultimately leading to a better understanding of how VA affects cirrus cloud properties and climate effects.

Moreover, our findings hold important scientific implications, particularly in the realm of cirrus cloud thinning (CCT) geoengineering (*61*, *62*). CCT involves intentionally inducing the negative-Twomey effect to mitigate the warming potential associated with cirrus clouds as explained by decreases in cloud albedo and emissivity due to increased effective radii and decreased ice number concentration and IWCs and increase in terrestrial radiation emitted to space. Despite its theoretical potential to combat global warming, CCT poses large uncertainties and risks. The National Academies of Sciences, Engineering, and Medicine (NASEM) have stressed the urgent need to advance our understanding of the feasibility, potential risks, and benefits of various solar climate intervention approaches (NASEM, 2021). Among these proposed strategies—such as stratospheric aerosol injection and marine cloud brightening—CCT remains the least studied. Our study contributes to this discourse by demonstrating the transformative impact of ash-rich eruptions on natural cirrus clouds, providing practical insight into this climate intervention technique that now lacks rigorous constraints. Furthermore, our observational analyses provide valuable constraints for validating and improving the representations of ice microphysics within climate models, which is critical for accurately predicting the radiative responses associated with such interventions.

Because of the remoteness of these three volcanoes, few in situ airborne and ground-based remote-sensing measurements were made.

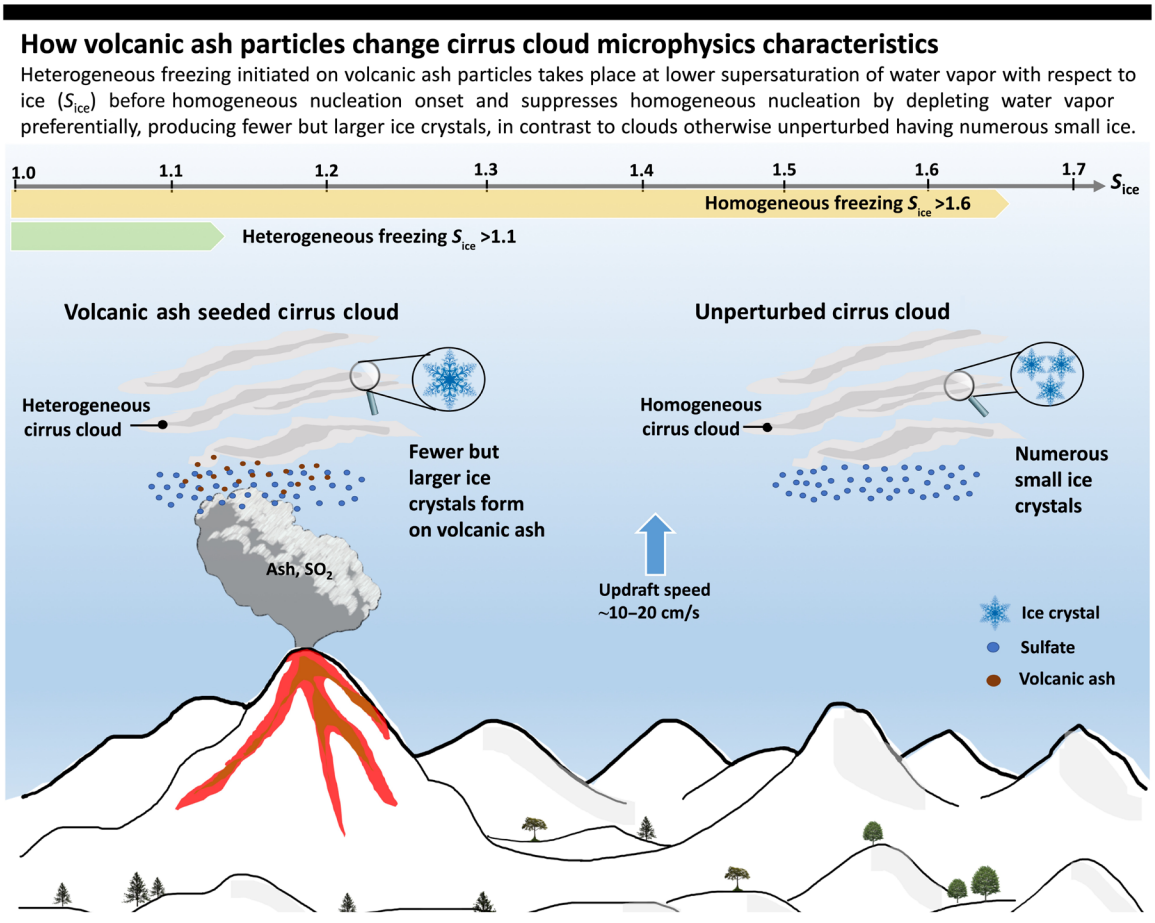

Fig. 5. Schematic illustrating how volcanic ash particles affect cirrus cloud microphysics. CREDIT: Illustration by L.L.

As a result, the satellite retrieval uncertainties of ice crystal number and radii are not quantified. Although associated with uncertainties, satellite remote-sensing fills in the gap to provide a large spatiotemporal coverage and long-term measurements of aerosols and clouds, which cannot be accomplished by balloon-borne and/or airborne in situ detailed measurements. Nevertheless, systematic errors of satellite retrievals are largely cancelled when taking differences between the volcanically perturbed and unperturbed periods. Random errors are also greatly suppressed by averaging over a geographical region of thousands of kilometers. Recognizing the limitations of satellite remote-sensing and associated data products based on which the analyses are conducted in this study, we emphasize that the trends in changes of ice cloud microphysical properties observed during the volcanic perturbed periods compared to the climatological mean are more robust than the absolute magnitudes. Multiple independent lines of evidence as well as VA abundance case contrast still enhance the credibility of the observed changes induced by volcanic aerosols. During future eruptions, in situ observations of aerosol and cloud properties as well as thermodynamic and dynamic conditions (e.g., temperature, humidity, and updraft velocity) obtained from dedicated field campaigns equipped with a unique payload aboard aircraft and balloons, in conjunction with ground-based and space-borne remote-sensing measurements are essential. By integrating these observational platforms with modeling studies for a targeted eruption, future research can better characterize the role of VA in cloud microphysics and improve our understanding of its impact on cirrus cloud formation and climate. This comprehensive approach will improve the accuracy of climate models to inform strategies for climate intervention and mitigation.

MATERIALS AND METHODS

CALIPSO L3 stratospheric aerosol profile

The level 3 stratospheric aerosol profile data product version 1.00, derived from optical measurements acquired by the Cloud–Aerosol Lidar with Orthogonal Polarization (CALIOP) instrument onboard the CALIPSO satellite, provides altitude-resolved stratospheric aerosol optical properties globally since 2006. This data product was made possible by raising the standard calibration altitude of CALIOP from the previously fixed 30 to 34 to 36 to 39 km, which addresses the aerosol contamination issue and enables proper retrievals of stratospheric aerosol backscatter and extinction in regions previously (but incorrectly) assumed to be aerosol free. This data product reports monthly mean profiles of total attenuated backscatter, particulate backscatter, aerosol extinction, and attenuated scattering ratios at 532 nm on a uniform horizontal grid with 5° latitude by 20° longitude spacing and a vertical resolution of 900 m at altitudes between 8.2 and 36.2 km. Given the low signal-to-noise ratio (SNR) in

the stratospheric retrievals, substantial spatiotemporal averaging of the measurements is required to reasonably depict the stratospheric aerosol distribution. Only nighttime data are used in the current version of data product for better SNR. Features associated with cirrus clouds and polar stratospheric clouds above the tropopause are readily removed, and only stratospheric aerosol layers are retained. The extinction coefficients in the "all-aerosol" mode are derived from the retrieved particulate backscatter profiles using a constant lidar ratio of 50 sr^{-1}.

This data product informs us of the major stratospheric perturbations over the globe resulting from strong volcanic eruptions and extreme smoke events in years of 2006–2017 (Fig. 1) and guides to select volcanic eruption events for this study.

CloudSat-CALIPSO L2 DARDAR-Nice

The DARDAR-Nice (liDAR-raDAR–number concentration of ICE particles) orbital product offers altitude-resolved estimates of ice crystal number concentration (N_i) from joint spaceborne cloud radar [Cloud Profiling Radar (CPR) onboard CloudSat] and lidar (CALIOP/CALIPSO) measurements, which are used to constrain moments of parameterized particle size distributions. Once constrained, these particle size distributions are integrated from three minimum size thresholds to provide N_i corresponding to ice crystals with $d > 5$, 25, and 100 μm. A thorough evaluation against theoretical considerations and multitudes of in situ measurements suggests that the most reliable DARDAR-Nice retrievals are found at temperatures below −30°C, as the retrievals are more accurate due to the dominance of unimodal ice crystal size distribution and reduced ambiguity in the cloud phase. Thus, the best-estimated DARDAR-Nice data support the intention of this study. Retrievals of N_i are provided along the CloudSat footprint (1.7 km) with a vertical resolution of 60 m. This data product is limited to clouds with IWC $>10^{-8}$ kg m^{-3}. Data are available 80°S to 80°N from 2006 to 2016 except 2011 and early 2012 when CloudSat suffered a battery failure. Extending this analysis beyond 2016 is not feasible due to instrumental issues and/or CloudSat-CALIPSO dislocation.

Retrievals of N_i now provide a key quantity for studying ice nucleation processes and aerosol-cloud interactions. In this work, a subset of the level 2 DARDAR-Nice data for stratospheric cirrus clouds spanning years 2007–2016 (with 2011 excluded) is used for analysis. Thus, clouds included in this study fulfill the criteria of (i) being classified as ice clouds, (ii) temperatures of cloudy pixels below −38°C, and (iii) above the tropopause. To examine the behaviors of cirrus in response to volcanic aerosols, we compile the orbital N_i data that are above the local tropopause and fall into the latitudinal zonal band between 50°N and 60°N during the volcanically perturbed period in year 2008 into monthly mean and median values for the Kasatochi volcanic eruption, in contrast to the N_i climatology in the unperturbed period of 2012–2016. Similarly, the N_i data that fall into the latitudinal zonal band between 40°N and 60°N during the volcanically perturbed period in year 2009 are analyzed for the Sarychev volcanic eruption, in contrast to the N_i climatology in the unperturbed years 2012–2016. The N_i data that fall into the latitudinal zonal band between 40°S and 60°S in year 2015 are considered for the Calbuco volcanic eruption, in contrast to the unperturbed years 2007–2014. This work presents results based on the N_i data corresponding to ice crystals with $d > 5$ μm if not otherwise specified. Ice number concentrations with a minimum size of 5 μm from the DARDAR-Nice are used in this study because the number concentrations of small ice particles are essential for studying initial ice formation in cirrus clouds. The PDFs of log10[N_i (cm^{-3})] are generated using an equal-interval bin width of 0.5 from −3 to 1.

A summary of the statistics including sampling number, mean, median, and SD for the selected volcanic eruption cases and the unperturbed references are presented in tables S2 to S4. Uncertainty in the CloudSat-CALIPSO retrievals can be decomposed into systematic errors and random errors. Random errors are greatly suppressed by averaging over a geographical region of thousands of kilometers, while systematic errors are largely cancelled when taking differences between the volcanically perturbed and unperturbed periods.

CloudSat-CALIPSO L2 2C-ICE

The CloudSat and CALIPSO Ice Cloud Property Product (2C-ICE) version R05 (*63*–*65*) contain estimates of IWC and ice crystal effective radius (r_{eff}) with a horizontal resolution of 1.7 km and a vertical resolution of 240 m. This data product combines inputs of measured radar reflectivity factor from the CloudSat CPR and measured attenuated backscatter coefficients at 532 nm from CALISPO lidar to constrain the ice cloud retrievals.

For this study, we use the quantities of IWC and r_{eff} from 2007–2016 for ice clouds above the local tropopause, same as the DARDAR-Nice N_i analysis for the three selected volcanic eruption cases. Only data that are of good quality (i.e., quality flag = 0) are included for analysis. The PDFs of r_{eff} are generated using an equal-interval bin width of 0.5 μm from 5 to 30 μm.

CALIPSO L2 vertical feature mask

CALIPSO level 2 vertical feature mask (VFM) V4.2 data product is used to qualitatively infer the presence of sulfate aerosol and VA particle over the geographical areas of interest with volcanic perturbations lasting for months. These VFM data describe the vertical and horizontal distribution of aerosol layers and classify each aerosol layer in the stratosphere into one of four aerosol subtypes including sulfate/other, VA, elevated smoke, and PSC aerosol based on threshold criteria of temperature, depolarization, color ratio, and layer-integrated attenuated backscatter (γ'). All layers with attenuated backscatter centroids above the local tropopause are classified as stratospheric aerosol layers. Thresholds for distinguishing the sulfate/other, VA, and elevated smoke subtypes were developed empirically from observations of six volcanic plume events and several smoke events which were observed to penetrate the tropopause. Weakly scattering layers or layers exceeding the γ' threshold but having low depolarization and low color ratio are classified as sulfate/other. Layers exceeding the γ' threshold and having high depolarization are classified as VA, while layers with moderate to low depolarization together with enhanced color ratio are classified as smoke. Depolarization ratio indicates the degree to which particles are nonspherical. That is, an elevated depolarization ratio unambiguously identifies nonspherical particles.

Most VA particles are aspherical in nature. However, Riley *et al.* (*66*) have shown that basaltic and andesitic VA is more nearly spherical (aspect ratio of 1.5 to 1.7) than rhyolitic ash (aspect ratio of 2.2). There might be some increases in smoke misclassifications where the depolarization ratio for some ash layers is just low enough to resemble that of depolarizing smoke. It is also possible for mixtures of ash and sulfate in the same airmass measured by CALIOP to be misclassified as smoke because of the collectively yield moderate values of depolarization ratio. The analysis by Tackett *et al.* (*36*) estimates that sulfate/ash mixtures are misclassified as smoke for nearly

one-third of these layers. We note that the three selected volcanic eruptions (2008 Kasatochi, 2009 Sarychev, and 2015 Calbuco) are the only outstanding contributors to stratospheric aerosol perturbation at midlatitudes at the time they occurred. Without any other known/reported smoke aerosol sources, the classified smoke aerosol during the respective eruption periods could very likely be VA embedded in sulfate aerosols and/or more spherical VA particles. Considering these uncertainties, we combine ash and smoke subtypes together for VA occurrence statistics.

Volcanic eruption cases and geographic regions for analysis

We target cirrus clouds at midlatitudes in the LMS because they are an ideal receptor of VA. The reasons are (i) LMS cirrus are the high-altitude clouds first in contact with falling VA; (ii) the descending branch of the stratospheric Brewer-Dobson circulation increases the chance of cirrus making contact with falling VA; (iii) VA stays airborne for a relatively longer period compared to VA in the troposphere, increasing the likelihood and detectability of VA exerting impacts on cirrus over time; (iv) VA becomes the dominant INPs and would magnify its impact in the LMS pristine environment; and (v) the possible interferences from tropospheric INPs (e.g., mineral dust) and convection are presumably negligible.

Volcanic eruptions over the tropics are not considered mainly because tropical stratospheric dynamics are unfavorable for studying aerosol-cirrus interactions. The ascending branch of the Brewer-Dobson circulation lifts volcanic plumes to higher altitudes above the tropical tropopause layer, which tend to be cloud free (*67*), resulting in a small chance of volcanic aerosol contact with cirrus cloud for an appreciable period of time. Moreover, the poleward dispersion of tropical volcanic plumes dilutes the concentration over vast areas, probably dimming the signal of volcanic aerosol impact on cirrus. Between 2007 and 2016 near the tropics, only the 2014 Kelud volcano erupted with ejection starting at around 19 km. See section 3.1.2 and figure 10 in (*34*) for the lofting and dilution of the volcanic plumes from the 2014 Kelud eruption (February 2014; 7.9°S, 112.3°E).

Observations of stratospheric aerosol from CALIPSO and cloud microphysics (DARDAR-Nice, 2C-ICE) from CloudSat and CALIPSO spanning 2007–2016 (with 2011 excluded) are used. Beyond 2016, data are unavailable because of issues associated with the CPR/CloudSat instrument. Owing to the missing data during 2011 and early 2012 when CPR/CloudSat was malfunctioning, impacts from the Nabro and Puyehue volcanic eruptions in 2011 cannot be examined. The eruptions of Kasatochi, Sarychev Peak, and Calbuco (Fig. 1 and table S1) during the analysis period of 2007–2016 become the only candidates for this study. They all occurred at midlatitudes and were found to have injected volcanic emissions directly into the lower stratosphere.

Kasatochi (52.18°N, 175.51°W), an island volcano along the Aleutian arc, erupted in a series of distinct explosive events on 7 to 8 August 2008, injecting SO_2 and ash up to ~18 km in altitude (*68*). In subsequent days, VA and SO_2 were observed spreading eastward over the Pacific by several infrared satellite sensors (*69*) including the Moderate Resolution Imaging Spectroradiometer, the Advanced Very High Resolution Radiometer, the Atmospheric Infrared Sounder (AIRS), the Infrared Atmospheric Sounding Interferometer (IASI), and the Ozone Monitoring Instrument. SO_2 circled around the Northern Hemisphere at least once and remained detectable in the atmosphere for at least a month (*70*). At that time, it was the largest injection of SO_2 into the atmosphere since the 1991 Hudson eruption, with SO_2 mass of 0.9 to 2.7 Tg (*71*). A 17-hour period of continuous ash emission with plume height > 10.5 km as determined from satellite images was followed by a third explosive event (*68*, *72*). Infrared satellite retrievals estimated total ash mass loadings of 0.3 to 0.5 Tg (*69*). The far-traveled VA particles were last reported airborne in the LMS on 24 September (*73*). A large phytoplankton blooms initiated by VA deposition in August 2008 over northeast Pacific demonstrates the abundance of VA from the Kasatochi eruption (*74*). Aerosol extinction eventually returned to near unperturbed levels by spring 2009 (fig. S1A).

Sarychev (48.09°N, 153.20°E), one of the most active volcanoes in the Kuril Islands chain (Russia), began to erupt on 11 June 2009 and erupted explosively between 12 and 16 June, directly injecting about 1.2 ± 0.2 Tg SO_2 and ashes into the LMS seen by the IASI (*71*, *75*, *76*). The resulting sulfate aerosol cloud, observed with the Optical Spectrograph and Infrared Imaging System limb-scanning instrument on the Odin satellite and CALIPSO lidar, completed one full circuit of the Northern Hemisphere by 30 June and persisted throughout the rest of 2009 (fig. S1B). Satellite data showed at least 21 discrete explosive events that sent ash plumes with total mass on the order of 300 kT (0.3 Tg) to altitudes of 5 to 1 km between 12 and 14 June (*75*). The widespread and far-reaching ash layers caused flight cancellations in the busy North Pacific region.

The Chilean volcano Calbuco (41.33°S, 72.61°W) began to erupt on 22 April 2015 with initial SO_2 and ash plumes reaching altitudes of 18 to 21 km, followed by a second huge explosion on 23 April with ash reported between 12 km and up to 20 km by the Buenos Aires Volcanic Ash Advisory Centre. About 0.2 to 0.4 Tg of SO_2 (*77*, *78*) was injected into the atmosphere of the Southern Hemisphere and spread zonally bounded between the subtropical and midlatitude dynamical barriers (*79*). The initial ash plumes dispersed in a northeasterly direction across Chile, Argentina, Brazil, and Uruguay (*79*, *80*), and VA particles were mainly found equatorward of 40°S (*36*) with the absence within our study domain (40°S to 60°S, Fig. 2A). In situ measurements by a lightweight optical particle counter over the Reunion Island site (*79*) on 19 May have shown particle effective radius of 0.17 ± 0.02 μm, indicating that the particles observed several weeks after the eruption are quite small. OMPS and lidar observations started to show a return to pre-eruption conditions in April 2016 (also see fig. S1C).

Satellite data poleward of 60° are not included in the present analyses in particular for the Calbuco analysis as conditions over Antarctica during the Southern Hemisphere winter (June to August) are conducive to polar stratospheric cloud formation. Data equatorward of 40° are also excluded to minimize potential interferences from low-latitude deep convection and the convection-lofted tropospheric aerosols [e.g., mineral dust and anthropogenic aerosols transport into the stratosphere via the Asian summer monsoon anticyclone (*81*)].

There are no other reported sources of perturbation (e.g., extreme smoke events and dust storms) to the upper troposphere and lower stratosphere at midlatitudes in years 2008–2009 in the Northern Hemisphere and in year 2015 in the Southern Hemisphere except the 2008 Kasatochi, 2009 Sarychev, and 2015 Calbuco volcanic eruptions. The stratospheric aerosol perturbations presumably are of pure volcanic origin.

Consideration and constraint on meteorological covariability

A complete picture of the behaviors of cirrus clouds in response to volcanic aerosols requires understanding the influence of meteorological

factors. For this, we analyze a set of key meteorological variables including temperature, relative humidity, water vapor mixing ratio, and vertical wind speed that are obtained from satellite observations and/or reanalyses to disentangle signals of VA's effects on cirrus clouds from the meteorological covariability of VA and cirrus clouds.

The DARDAR-Nice data product provides the N_i-collocated temperature information that is obtained by interpolation to each satellite track from the ancillary European Center for Medium-Range Weather Forecasts (ECMWF) state variable dataset. This collocated pair of N_i and temperature is used to tease out aerosol-cloud interactions from the meteorological covariations for the three volcanic perturbed cases. A wide range of cirrus-relevant temperatures is divided with an equal-interval bin width of 2°C from −34° to −80°C. We compare N_i during the volcanically perturbed versus the unperturbed periods for different temperatures (fig. S21). See section S3.

Temperature, relative humidity, and vertical wind speed obtained from (i) the final analysis reanalysis data product of the National Centers for Environmental Prediction (NCEP) (horizontal resolution of 1° × 1°; temporal resolution of 6 hours) and (ii) the ECMWF release of the fifth generation of reanalysis (ERA5) (horizontal resolution of 0.25° × 0.25°; temporal resolution of monthly) are analyzed in the same manner as the cirrus microphysics analyses. That is, data from 2007–2016 at both hemispheric midlatitudes are considered to contrast the meteorological conditions during the volcanically perturbed versus the unperturbed periods, aiming to demonstrate the similarity between the two periods and deny meteorological covariations.

The MLS (Microwave Limb Sounder) onboard NASA's Earth Observing System (EOS) Aura satellite and the AIRS onboard NASA's EOS Aqua satellite report profiles of water vapor (H_2O) concentrations, temperature, and relative humidity. We contrast these meteorological factors between the volcanically perturbed versus the unperturbed periods, same as the cirrus microphysics analyses.

Calculation of tropopause

The altitude of the lapse-rate tropopause is estimated using temperature and geopotential height variables from the ERA5 reanalysis on a 0.75° × 0.75° longitude-latitude grid. The tropopause altitude is calculated by first linearly interpolating temperatures in each column to a regular 250-m-altitude grid and then applying the World Meteorological Organization (WMO) tropopause definition (*82*). Here, we use the lowest (primary) tropopause. For validation of the quality of tropopause altitudes derived from gridded reanalyses, see, e.g., (*83*–*85*). Aerosol and cloud properties above the tropopause are obtained by collocating other datasets to this tropopause dataset.

Parcel model simulations

Our objective is to investigate the effect of heterogeneous ice nucleation on VA particles on ice crystal number concentrations. On the basis of a cloud parcel model with homogeneous freezing of aqueous sulfate aerosols (*86*), we further formulate the heterogeneous ice nucleation on VA particles and the competing effects of homogeneous and heterogeneous freezing in the LMS scenario. The microphysical ice nucleation processes implemented are as follows: The homogeneous freezing rate calculated on the basis of the water activity parameterization after Koop *et al.* (*87*) is used. Homogeneous freezing is independent of the chemical nature of the solution but depends only on the water activity of the solution droplets. Sulfate aerosols in the upper troposphere and lower stratosphere are soluble especially at high relative humidities required for homogeneous ice nucleation. We thus assume that sulfate particles form ice through homogeneous freezing after deliquescence. For the representation of heterogeneous nucleation on VA particles in the deposition freezing mode, we use the experiment-derived parameterization of ash active surface site density as a function of temperature and RH_{ice} (*10*), with the ice nucleation efficiency quantified in terms of the ice active surface site density approach. The deposition ice nucleation parameterization is derived from data for 224 K < T < 234 K. A fundamental assumption made is that the ice nucleation activity of VA particles in the upper troposphere and the lower stratosphere is in principle robustly represented by the laboratory experiments on ash samples. The high silica contents found in VA particles (*8*, *10*, *11*) suggest that they are in general chemically akin to certain mineral dust particles (e.g. Saharan dust). As expected, the VA samples collected from different volcanoes were found to initiate deposition nucleation at least comparatively to or more efficiently than the Asian and Saharan dust. A comparison of the ice nucleation active surface site densities between VA and desert dust for deposition ice nucleation is shown in fig. S25. Likely exposed to additional chemical processing in the presence of abundant sulfuric acid during eruption, VA particles might be internally mixed with sulfuric acid to a varying degree, and some laboratory studies indicate that thick coatings of sulfate content reduce their nucleation efficiency. However, direct measurements of VA particles being coated by sulfuric acid are missing. We note that the objective of our modeling analysis is to provide a conceptual framework that explains observational results. We do not aim to determine the dominant heterogeneous ice nucleation mechanism in cirrus clouds which depends on whether ash particles are coated by sulfate and the weight percent of sulfate on ash particles. An assumption made in the modeling section here is that the ice nucleation activity of VA particles in the upper troposphere and the lower stratosphere is in principle represented by the laboratory experiments on ash samples analyzed by Steinke *et al.* (*10*).

Individual simulations are driven by constant updraft speeds representative of mesoscale gravity wave dynamics. As an air parcel ascends, it cools adiabatically before water vapor phase transforms and the supersaturation over ice (S_{ice}) increases. Heterogeneous nucleation on VA particles takes place when S_{ice} > 0.1 to produce the first ice crystals. After nucleation, further microphysical processes consider the diffusional growth of both newly nucleated and preexisting ice crystals to deplete water vapor and reduce S_{ice}. Processes that affect ice number concentrations, such as sedimentation, aggregation, and entrainment, are not included. Sensitivity experiments in which sedimentation of both homogeneously and heterogeneously induced ice is considered are conducted to confirm that considering sedimentation does not change the conclusions of this study. As VA INP concentration increases and for conditions less favorable for homogeneous ice nucleation (e.g., relatively high temperatures and slow updrafts), sedimentation starts to play a negligible role. If ice crystals firstly nucleated on VA particles are abundant and the updraft is slow, then depositional growth of the ice crystals will consume water vapor sufficiently and prevent S_{ice} from rising toward the threshold for homogeneous freezing. In this case, homogeneous freezing is suppressed, and the ice number concentration is mostly determined by the abundance of VA nuclei. On the other hand, for low concentrations of VA particles and strong updraft, depositional growth of heterogeneously nucleated ice would not consume water vapor rapidly, and heterogeneous freezing events are succeeded by homogeneous freezing as S_{ice} threshold for homogeneous freezing

can be reached. Under this circumstance, homogeneous freezing dominates the ice concentration. When pure homogeneous freezing is enabled or at low VA concentrations, simulation results tend to represent the characteristics of cirrus for the ash-poor scenario (Fig. 4A and the leftmost of Fig. 4B), whereas with increasing VA concentrations, simulation results are more representative of cirrus for the ash-rich scenario (on the right of Fig. 4B).

Aqueous sulfate aerosols are represented by a log-normal size distribution with a mode radius of 0.2 μm, a distribution width of 2.3, and a total number concentration of 200 cm^{-3}. Results show small sensitivity to the aqueous aerosol size distribution and their concentration. High-altitude measurements conducted following the eruptions of Mount St. Helens in 1980, El Chichon in 1982, and Mt. Kelud in 2014 revealed a wide size distribution of VA particles injected into the stratosphere (*38*, *39*, *43*). Meanwhile, atmospheric measurements of VA particle size distribution are meager. For this reason, an ensemble of sensitivity experiments is conducted to take into account a large range of spread in VA particle size distribution. VA particles are represented by a log-normal size distribution with mode radii ranging from 0.1 to 0.8 μm (*38*), the SD ranging from 1.2 to 1.8, and the total number concentration ranging from 1 to 3000 $liter^{-1}$. Aqueous sulfate aerosols and VA particles are depleted from the size distribution as homogeneous and heterogeneous nucleation, respectively, takes place. Our parcel model is initialized by aerosol size distributions and number concentration and is driven by temperature and pressure changes. We keep track of the nucleation and growth of ice crystals and the changes in water vapor and temperature. If S_{ice} is decreased to 0.01 below the maximum S_{ice} during a simulation, then parcel model simulation stops. Results show that simulated ice crystal number concentrations are strongly sensitive to the VA nuclei concentration particularly for slow updraft and high temperature. VA particle concentration as low as 10 $liter^{-1}$ already suppresses homogeneous freezing at updraft speed of 10 to 20 cm s^{-1}, and nucleation on ash particles dominates ice number concentration (fig. S26).

Large VA particles exhibit high fall velocities, causing them to rapidly exit the stratosphere. Smaller ash particles contribute to the longer-lasting stratospheric volcanic aerosols. Ash particles with maximum dimensions of a few microns persisted for 6 months to a year after the El Chichon eruption [Volcanic Explosivity Index (VEI) = 5] (*39*). Vernier *et al.* (*41*) suggested that submicrometer VA particles from the tropical Mt. Kelut eruption contribute to an aerosol layer observed to persist for 3 months. Fine ash particles have an atmospheric lifetime that can span months (~0.01 km/hour) (*88*, *89*). Numerical simulations by Turco *et al.* (*90*) indicate that particles larger than about 5 μm in diameter will be removed from the stratosphere by sedimentation within a few weeks. Therefore, our investigation focuses on testing the influence of submicrometer VA particles. Moreover, large ash particles have large surface areas, making them more effective initiators of ice nucleation than smaller ones. Assuming VA particles of comparable size to sulfate aerosols provides an upper limit for the minimum amount of VA needed to inhibit homogeneous freezing.

Supplementary Materials

This PDF file includes:

Supplementary Text S1 to S3
Figs. S1 to S26
Tables S1 to S4
References

REFERENCES AND NOTES

1. K.-N. Liou, Influence of cirrus clouds on weather and climate processes: A global perspective. *Mon. Weather Rev.* **114**, 1167–1199 (1986).
2. Q. Fu, K.-N. Liou, Parameterization of the radiative properties of cirrus clouds. *J. Atmos. Sci.* **50**, 2008–2025 (1993).
3. B. J. Murray, X. Liu, "Ice-nucleating particles and their effects on clouds and radiation" in *Aerosols and Climate*, K. S. Carslaw, Ed. (Elsevier, 2022), pp. 619–649.
4. K. Isono, M. Komabayasi, A. Ono, Volcanoes as a source of atmospheric ice nuclei. *Nature* **183**, 317–318 (1959).
5. P. V. Hobbs, C. M. Fullerton, G. C. Bluhm, Ice nucleus storms in Hawaii. *Nature* **230**, 90–91 (1971).
6. A. P. Fornea, S. D. Brooks, J. B. Dooley, A. Saha, Heterogeneous freezing of ice on atmospheric aerosols containing ash, soot, and soil. *J. Geophys. Res.* **114**, D13201 (2009).
7. N. S. Umo, R. Ullrich, E. C. Maters, I. Steinke, N. Benker, K. Höhler, R. Wagner, P. G. Weidler, G. A. Hoshyaripour, A. Kiselev, U. Kueppers, K. Kandler, D. B. Dingwell, T. Leisner, O. Möhler, The influence of chemical and mineral compositions on the parameterization of immersion freezing by volcanic ash particles. *J. Geophys. Res. Atmos.* **126**, e2020JD033356 (2021).
8. C. R. Hoyle, V. Pinti, A. Welti, B. Zobrist, C. Marcolli, B. Luo, Á. Höskuldsson, H. B. Mattsson, O. Stetzer, T. Thorsteinsson, G. Larsen, T. Peter, Ice nucleation properties of volcanic ash from Eyjafjallajökull. *Atmos. Chem. Phys.* **11**, 9911–9926 (2011).
9. B. J. Murray, D. O'Sullivan, J. D. Atkinson, M. E. Webb, Ice nucleation by particles immersed in supercooled cloud droplets. *Chem. Soc. Rev.* **41**, 6519–6554 (2012).
10. I. Steinke, O. Möhler, A. Kiselev, M. Niemand, H. Saathoff, M. Schnaiter, J. Skrotzki, C. Hoose, T. Leisner, Ice nucleation properties of fine ash particles from the Eyjafjallajökull eruption in April 2010. *Atmos. Chem. Phys.* **11**, 12945–12958 (2011).
11. G. P. Schill, K. Genareau, M. A. Tolbert, Deposition and immersion-mode nucleation of ice by three distinct samples of volcanic ash. *Atmos. Chem. Phys.* **15**, 7523–7536 (2015).
12. J. R. Campbell, E. J. Welton, N. A. Krotkov, K. Yang, S. A. Stewart, M. D. Fromm, Likely seeding of cirrus clouds by stratospheric Kasatochi volcanic aerosol particles near a mid-latitude tropopause fold. *Atmos. Environ.* **46**, 441–448 (2012).
13. P. Seifert, A. Ansmann, S. Groß, V. Freudenthaler, B. Heinold, A. Hiebsch, I. Mattis, J. Schmidt, F. Schnell, M. Tesche, U. Wandinger, M. Wiegner, Ice formation in ash-influenced clouds after the eruption of the Eyjafjallajökull volcano in April 2010. *J. Geophys. Res.* **116**, D00U04 (2011).
14. C. Rolf, M. Krämer, C. Schiller, M. Hildebrandt, M. Riese, Lidar observation and model simulation of a volcanic-ash-induced cirrus cloud during the Eyjafjallajökull eruption. *Atmos. Chem. Phys.* **12**, 10281–10294 (2012).
15. K. Gierens, On the transition between heterogeneous and homogeneous freezing. *Atmos. Chem. Phys.* **3**, 437–446 (2003).
16. B. Kärcher, P. J. DeMott, E. J. Jensen, J. Y. Harrington, Studies on the competition between homogeneous and heterogeneous ice nucleation in cirrus formation. *J. Geophys. Res. Atmos.* **127**, e2021JD035805 (2022).
17. B. Kärcher, A parameterization of cirrus cloud formation: Revisiting competing ice nucleation. *J. Geophys. Res.-Atmos.* **127**, e2022JD036907 (2022).
18. W. Haag, B. Kärcher, The impact of aerosols and gravity waves on cirrus clouds at midlatitudes. *J. Geophys. Res.* **109**, D12202 (2004).
19. H. Pruppacher, J. Klett, "Heterogeneous nucleation" in *Microphysics of Clouds and Precipitation, Atmospheric and Oceanographic Sciences Library* (Springer, 2010), vol. 18.
20. P. J. DeMott, D. C. Rogers, S. M. Kreidenweis, Y. Chen, C. H. Twohy, D. Baumgardner, A. J. Heymsfield, K. R. Chan, The role of heterogeneous freezing nucleation in upper tropospheric clouds: Inferences from SUCCESS. *Geophys. Res. Lett.* **25**, 1387–1390 (1998).
21. B. Kärcher, U. Lohmann, A parameterization of cirrus cloud formation: Heterogeneous freezing. *J. Geophys. Res.* **108**, 4402 (2003).
22. P. Spichtinger, D. J. Cziczo, Impact of heterogeneous ice nuclei on homogeneous freezing events in cirrus clouds. *J. Geophys. Res. Atmos.* **115**, D14208 (2010).
23. S. Twomey, Pollution and the planetary albedo. *Atmos. Environ.* **8**, 1251–1256 (1974).
24. C. E. Junge, C. W. Chagnon, J. E. Manson, A world-wide stratospheric aerosol layer. *Science* **133**, 1478–1479 (1961).
25. R. P. Turco, R. C. Whitten, O. B. Toon, Stratospheric aerosols: Observation and theory. *Rev. Geophys.* **20**, 233–279 (1982).
26. T. Deshler, M. E. Hervig, D. J. Hofmann, J. M. Rosen, J. B. Liley, Thirty years of in situ stratospheric aerosol size distribution measurements from Laramie, Wyoming (41°N), using balloon-borne instruments. *J. Geophys. Res.* **108**, 4167 (2003).
27. T. Deshler, A review of global stratospheric aerosol: Measurements, importance, life cycle, and local stratospheric aerosol. *Atmos. Res.* **90**, 223–232 (2008).
28. S. Kremser, L. W. Thomason, M. von Hobe, M. Hermann, T. Deshler, C. Timmreck, M. Toohey, A. Stenke, J. P. Schwarz, R. Weigel, S. Fueglistaler, F. J. Prata, J.-P. Vernier, H. Schlager, J. E. Barnes, J.-C. Antuña-Marrero, D. Fairlie, M. Palm, E. Mahieu, J. Notholt, M. Rex, C. Bingen, F. Vanhellemont, A. Bourassa, J. M. C. Plane, D. Klocke, S. A. Carn,

L. Clarisse, T. Trickl, R. Neely, A. D. James, L. Rieger, J. C. Wilson, B. Meland, Stratospheric aerosol—Observations, processes, and impact on climate. *Rev. Geophys.* **54**, 278–335 (2016).
29. A. Podglajen, A. Hertzog, R. Plougonven, B. Legras, Lagrangian temperature and vertical velocity fluctuations due to gravity waves in the lower stratosphere. *Geophys. Res. Lett.* **43**, 3543–3553 (2016).
30. B. Kärcher, A. Podglajen, A stochastic representation of temperature fluctuations induced by mesoscale gravity waves. *J. Geophys. Res.* **124**, 11506–11529 (2019).
31. B. Kärcher, E. J. Jensen, U. Lohmann, The impact of mesoscale gravity waves on homogeneous ice nucleation in cirrus clouds. *Geophys. Res. Lett.* **46**, 5556–5565 (2019).
32. B. Kärcher, C. Marcolli, F. Mahrt, The role of mineral dust aerosol particles in aviation soot-cirrus interactions. *J. Geophys. Res.* **128**, e2022JD37881 (2023).
33. J. Kar, M. A. Vaughan, K.-P. Lee, J. L. Tackett, M. A. Avery, A. Garnier, B. J. Getzewich, W. H. Hunt, D. Josset, Z. Liu, P. L. Lucker, B. Magill, A. H. Omar, J. Pelon, R. R. Rogers, T. D. Toth, C. R. Trepte, J.-P. Vernier, D. M. Winker, S. A. Young, CALIPSO lidar calibration at 532 nm: Version 4 nighttime algorithm. *Atmos. Meas. Tech.* **11**, 1459–1479 (2018).
34. J. Kar, K.-P. Lee, M. A. Vaughan, J. L. Tackett, C. R. Trepte, D. M. Winker, P. L. Lucker, B. J. Getzewich, CALIPSO level 3 stratospheric aerosol profile product: Version 1.00 algorithm description and initial assessment. *Atmos. Meas. Tech.* **12**, 6173–6191 (2019).
35. A. T. Prata, S. A. Young, S. T. Siems, M. J. Manton, Lidar ratios of stratospheric volcanic ash and sulfate aerosols retrieved from CALIOP measurements. *Atmos. Chem. Phys.* **17**, 8599–8618 (2017).
36. J. L. Tackett, J. Kar, M. A. Vaughan, B. J. Getzewich, M.-H. Kim, J.-P. Vernier, A. H. Omar, B. E. Magill, M. C. Pitts, D. M. Winker, The CALIPSO version 4.5 stratospheric aerosol subtyping algorithm. *Atmos. Meas. Tech.* **16**, 745–768 (2023).
37. O. Sourdeval, E. Gryspeerdt, M. Krämer, T. Goren, J. Delanoë, A. Afchine, F. Hemmer, J. Quaas, Ice crystal number concentration estimates from lidar–radar satellite remote sensing – Part 1: Method and evaluation. *Atmos. Chem. Phys.* **18**, 14327–14350 (2018).
38. N. H. Farlow, V. R. Oberbeck, K. G. Snetsinger, G. V. Ferry, G. Polkowski, D. M. Hayes, Size distributions and mineralogy of ash particles in the stratosphere from eruptions of Mount St. Helens. *Science* **211**, 832–834 (1981).
39. J. L. Gooding, U. S. Clanton, E. M. Gabel, J. L. Warren, El Chichón volcanic ash in the stratosphere: Particle abundances and size distributions after the 1982 eruption. *Geophys. Res. Lett.* **10**, 1033–1036 (1983).
40. G. Vaughan, D. P. Wareing, S. B. Jones, L. Thomas, N. Larsen, Lidar measurements of Mt. Pinatubo aerosols at Aberystwyth from August 1991 through March 1992. *Geophys. Res. Lett.* **21**, 1315–1318 (1994).
41. J.-P. Vernier, T. D. Fairlie, T. Deshler, M. Natarajan, T. Knepp, K. Foster, F. G. Wienhold, K. M. Bedka, L. Thomason, C. Trepte, In situ and space-based observations of the Kelud volcanic plume: The persistence of ash in the lower stratosphere. *J. Geophys. Res. Atmos.* **121**, 11104–11118 (2016).
42. E. J. Jensen, S. Woods, R. P. Lawson, T. P. Bui, L. Pfister, T. D. Thornberry, A. W. Rollins, J.-P. Vernier, L. L. Pan, S. Honomichl, O. B. Toon, Ash particles detected in the tropical lower stratosphere. *Geophys. Res. Lett.* **45**, 11483–11489 (2018).
43. Y. Zhu, O. B. Toon, E. J. Jensen, C. G. Bardeen, M. J. Mills, M. A. Tolbert, P. Yu, S. Woods, Persisting volcanic ash particles impact stratospheric SO_2 lifetime and aerosol optical properties. *Nat. Commun.* **11**, 4526 (2020).
44. A. Cirisan, P. Spichtinger, B. P. Luo, D. K. Weisenstein, H. Wernli, U. Lohmann, T. Peter, Microphysical and radiative changes in cirrus clouds by geoengineering the stratosphere: Geoengineering effect on cirrus clouds. *J. Geophys. Res. Atmos.* **118**, 4533–4548 (2013).
45. B. Zhao, Y. Wang, Y. Gu, K.-N. Liou, J. H. Jiang, J. Fan, X. Liu, L. Huang, Y. L. Yung, Ice nucleation by aerosols from anthropogenic pollution. *Nat. Geosci.* **12**, 602–607 (2019).
46. C. J. Williamson, A. Kupc, A. Rollins, J. Kazil, K. D. Froyd, E. A. Ray, D. M. Murphy, G. P. Schill, J. Peischl, C. Thompson, I. Bourgeois, T. B. Ryerson, G. S. Diskin, J. P. DiGangi, D. R. Blake, T. P. V. Bui, M. Dollner, B. Weinzierl, C. A. Brock, Large hemispheric difference in nucleation mode aerosol concentrations in the lowermost stratosphere at mid- and high latitudes. *Atmos. Chem. Phys.* **21**, 9065–9088 (2021).
47. F. Yu, G. Luo, A. A. Nair, S. Eastham, C. J. Williamson, A. Kupc, C. A. Brock, Particle number concentrations and size distributions in the stratosphere: Implications of nucleation mechanisms and particle microphysics. *Atmos. Chem. Phys.* **23**, 1863–1877 (2023).
48. B. Kärcher, U. Lohmann, A parameterization of cirrus cloud formation: Homogeneous freezing including effects of aerosol size. *J. Geophys. Res. Atmos.* **107**, AAC 4-1–AAC 4-10 (2002).
49. X. Liu, J. E. Penner, Ice nucleation parameterization for global models. *Meteorol. Z.* **14**, 499–514 (2005).
50. X. Liu, X. Shi, Sensitivity of homogeneous ice nucleation to aerosol perturbations and its implications for aerosol indirect effects through cirrus clouds. *Geophys. Res. Lett.* **45**, 1684–1691 (2018).
51. E. J. Jensen, O. B. Toon, The potential effects of volcanic aerosols on cirrus cloud microphysics. *Geophys. Res. Lett.* **19**, 1759–1762 (1992).
52. A. J. Durant, R. A. Shaw, W. I. Rose, Y. Mi, G. G. J. Ernst, Ice nucleation and overseeding of ice in volcanic clouds. *J. Geophys. Res. Atmos.* **113**, D09206 (2008).
53. M. McCormick, L. Thomason, C. Trepte, Atmospheric effects of the Mt Pinatubo eruption. *Nature* **373**, 399–404 (1995).
54. F. F. Malavelle, J. M. Haywood, A. Jones, A. Gettelman, L. Clarisse, S. Bauduin, R. P. Allan, I. H. H. Karset, J. E. Kristjánsson, L. Oreopoulos, N. Cho, D. Lee, N. Bellouin, O. Boucher, D. P. Grosvenor, K. S. Carslaw, S. Dhomse, G. W. Mann, A. Schmidt, H. Coe, M. E. Hartley, M. Dalvi, A. A. Hill, B. T. Johnson, C. E. Johnson, J. R. Knight, F. M. O'Connor, D. G. Partridge, P. Stier, G. Myhre, S. Platnick, G. L. Stephens, H. Takahashi, T. Thordarson, Strong constraints on aerosol–cloud interactions from volcanic eruptions. *Nature* **546**, 485–491 (2017).
55. Y. Chen, J. Haywood, Y. Wang, F. Malavelle, G. Jordan, D. Partridge, J. Fieldsend, J. De Leeuw, A. Schmidt, N. Cho, L. Oreopoulos, S. Platnick, D. Grosvenor, P. Field, U. Lohmann, Machine learning reveals climate forcing from aerosols is dominated by increased cloud cover. *Nat. Geosci.* **15**, 609–614 (2022).
56. C. E. Sioris, A. Malo, C. A. McLinden, R. D'Amours, Direct injection of water vapor into the stratosphere by volcanic eruptions. *Geophys. Res. Lett.* **43**, 7694–7700 (2016).
57. X. Liu, J. E. Penner, Effect of Mount Pinatubo H_2SO_4/H_2O aerosol on ice nucleation in the upper troposphere using a global chemistry and transport model. *J. Geophys. Res.* **107**, AAC 2-1–AAC 2-18 (2002).
58. U. Lohmann, B. Kärcher, C. Timmreck, Impact of the Mount Pinatubo eruption on cirrus clouds formed by homogeneous freezing in the ECHAM4 GCM. *J. Geophys. Res.* **108**, 4568 (2003).
59. A. F. Wells, A. Jones, M. Osborne, L. Damany-Pearce, D. G. Partridge, J. M. Haywood, Including ash in UKESM1 model simulations of the Raikoke volcanic eruption reveals improved agreement with observations. *Atmos. Chem. Phys.* **23**, 3985–4007 (2023).
60. S. C. Sullivan, D. M. Lee, L. Oreopoulos, A. Nenes, Role of updraft velocity in temporal variability of global cloud hydrometeor number. *Proc. Natl. Acad. Sci. U.S.A.* **113**, 5791–5796 (2016).
61. D. L. Mitchell, W. Finnegan, Modification of cirrus clouds to reduce global warming. *Env. Res. Lett.* **4**, 045102 (2009).
62. U. Lohmann, B. Gasparini, A cirrus cloud climate dial? *Science* **357**, 248–249 (2017).
63. M. Deng, G. G. Mace, Z. Wang, E. Berry, CloudSat 2C-ICE product update with a new Ze parameterization in lidar-only region. *J. Geophys. Res. Atmos.* **120**, 12198–12208 (2015).
64. M. Deng, G. G. Mace, Z. Wang, P. Lawson, Evaluation of several A-train ice cloud retrieval products with in situ measurements collected during the SPARTICUS campaign. *J. Appl. Meteor. Climatol.* **52**, 1014–1030 (2013).
65. M. Deng, G. G. Mace, Z. Wang, H. Okamoto, Tropical composition, cloud and climate coupling experiment validation for cirrus cloud profiling retrieval using CloudSat radar and CALIPSO lidar. *J. Geophys. Res.* **115**, D00J15 (2010).
66. C. M. Riley, W. I. Rose, G. J. S. Bluth, Quantitative shape measurements of distal volcanic ash. *J. Geophys. Res.* **108**, 2504 (2003).
67. Q. Fu, Y. Hu, Q. Yang, Identifying the top of the tropical tropopause layer from vertical mass flux analysis and CALIPSO lidar cloud observations. *Geophys. Res. Lett.* **34**, L14813 (2007).
68. C. F. Waythomas, W. E. Scott, S. G. Prejean, D. J. Schneider, P. Izbekov, C. J. Nye, The 7–8 August 2008 eruption of Kasatochi Volcano, central Aleutian Islands, Alaska. *J. Geophys. Res.* **115**, B00B06 (2010).
69. S. Corradini, L. Merucci, A. J. Prata, A. Piscini, Volcanic ash and SO2 in the 2008 Kasatochi eruption: Retrievals comparison from different IR satellite sensors. *J. Geophys. Res.* **115**, D00L21 (2010).
70. N. A. Krotkov, M. R. Schoeberl, G. A. Morris, S. Carn, K. Yang, Dispersion and lifetime of the SO_2 cloud from the August 2008 Kasatochi eruption. *J. Geophys. Res.* **115**, D00L20 (2010).
71. S. A. Carn, L. Clarisse, A. J. Prata, Multi-decadal satellite measurements of global volcanic degassing. *J. Volcanol. Geotherm. Res.* **311**, 99–134 (2016).
72. C. A. Neal, R. G. McGimsey, J. P. Dixon, C. E. Cameron, A. A. Nuzhdaev, M. Chivisova, 2008 Volcanic activity in Alaska, Kamchatka, and the Kurile Islands: Summary of events and response of the Alaska Volcano Observatory, U.S. Geological Survey Scientific Investigations Report 2010-5243 (2011), 94 p.
73. A. Hoffmann, C. Ritter, M. Stock, M. Maturilli, S. Eckhardt, A. Herber, R. Neuber, Lidar measurements of the Kasatochi aerosol plume in August and September 2008 in Ny-Ålesund, Spitsbergen. *J. Geophys. Res.* **115**, D00L12 (2010).
74. R. C. Hamme, P. W. Webley, W. R. Crawford, F. A. Whitney, M. D. DeGrandpre, S. R. Emerson, C. C. Eriksen, K. E. Giesbrecht, J. F. R. Gower, M. T. Kavanaugh, M. A. Peña, C. L. Sabine, S. D. Batten, L. A. Coogan, D. S. Grundle, D. Lockwood, Volcanic ash fuels anomalous plankton bloom in subarctic northeast Pacific. *Geophys. Res. Lett.* **37**, L19604 (2010).
75. A. Rybin, M. Chibisova, P. Webley, T. Steensen, P. Izbekov, C. A. Neal, V. Realmuto, Satellite and ground observations of the June 2009 eruption of Sarychev Peak volcano, Matua Island, Central Kuriles. *Bull. Volcanol.* **73**, 1377–1392 (2011).
76. J. M. Haywood, A. Jones, L. Clarisse, A. Bourassa, J. Barnes, P. Telford, N. Bellouin, O. Boucher, P. Agnew, C. Clerbaux, P. Coheur, D. Degenstein, P. Braesicke, Observations of the eruption of the Sarychev volcano and simulations using the HadGEM2 climate model. *J. Geophys. Res.* **115**, D21212 (2010).

77. F. Pardini, M. Burton, F. Arzilli, G. La Spina, M. Polacci, SO_2 emissions, plume heights, and magmatic processes inferred from satellite data: The 2015 Calbuco eruptions. *J. Volcanol. Geotherm. Res.* **361**, 12–24 (2018).
78. Y. Zhu, O. B. Toon, D. Kinnison, V. L. Harvey, M. J. Mills, C. G. Bardeen, M. Pitts, N. Bègue, J.-B. Renard, G. Berthet, F. Jégou, Stratospheric aerosols, polar stratospheric clouds, and polar ozone depletion after the Mount Calbuco Eruption in 2015. *J. Geophys. Res.-Atmos.* **123**, 12308–12331 (2018).
79. N. Bègue, D. Vignelles, G. Berthet, T. Portafaix, G. Payen, F. Jégou, H. Benchérif, J. Jumelet, J.-P. Vernier, T. Lurton, J.-B. Renard, L. Clarisse, V. Duverger, F. Posny, J.-M. Metzger, S. Godin-Beekmann, Long-range transport of stratospheric aerosols in the Southern Hemisphere following the 2015 Calbuco eruption. *Atmos. Chem. Phys.* **17**, 15019–15036 (2017).
80. F. J. S. Lopes, J. J. Silva, J. C. Antuña Marrero, G. Taha, E. Landulfo, Synergetic aerosol layer observation after the 2015 Calbuco volcanic eruption event. *Remote Sens.* **11**, 195 (2019).
81. X. Wu, Q. Qiao, B. Chen, X. Wang, L. Hoffmann, S. Griessbach, Y. Tian, Y. Wang, The influence of the Asian summer monsoon on volcanic aerosol transport in the UTLS region. *NPJ Clim. Atmos. Sci.* **6**, 11 (2023).
82. World Meteorological Organization: Definition of the tropopause, *Bulletin of the World Meteorological Organization*, **6**, 136–137 (1957).
83. T. Reichler, M. Dameris, R. Sausen, Determining the tropopause height from gridded data. *Geophys. Res. Lett.* **30**, 2042 (2003).
84. D. L. Solomon, K. P. Bowman, C. R. Homeyer, Tropopause-penetrating convection from three-dimensional gridded NEXRAD data. *J. Appl. Meteor. Climatol.* **55**, 465–478 (2016).
85. S. Tegtmeier, J. Anstey, S. Davis, R. Dragani, Y. Harada, I. Ivanciu, R. Pilch Kedzierski, K. Krüger, B. Legras, C. Long, J. S. Wang, K. Wargan, J. S. Wright, Temperature and tropopause characteristics from reanalyses data in the tropical tropopause layer. *Atmos. Chem. Phys.* **20**, 753–770 (2020).
86. X. Shi, X. Liu, Effect of cloud-scale vertical velocity on the contribution of homogeneous nucleation to cirrus formation and radiative forcing. *Geophys. Res. Lett.* **43**, 6588–6595 (2016).
87. T. Koop, B. Luo, A. Tsias, T. Peter, Water activity as the determinant for homogeneous ice nucleation in aqueous solutions. *Nature* **406**, 611–614 (2000).
88. C. Bonadonna, G. G. J. Ernst, R. S. J. Sparks, Thickness variations and volume estimates of tephra fall deposits; the importance of particle Reynolds number. *J. Volcanol. Geotherm. Res.* **81**, 173–187 (1998).
89. A. J. Durant, Toward a realistic formulation of fine-ash lifetime in volcanic clouds. *Res. Focus* **43**, 271–272 (2015).
90. R. P. Turco, O. B. Toon, T. P. Ackerman, J. B. Pollack, C. Sagan, Nuclear winter: Global consequences of multiple explosions. *Science* **222**, 4630 (1983).
91. M. Krämer, C. Rolf, A. Luebke, A. Afchine, N. Spelten, A. Costa, J. Meyer, M. Zöger, J. Smith, R. L. Herman, B. Buchholz, V. Ebert, D. Baumgardner, S. Borrmann, M. Klingebiel, L. Avallone, A microphysics guide to cirrus clouds—Part 1: Cirrus types. *Atmos. Chem. Phys.* **16**, 3463–3483 (2016).
92. M. Krämer, C. Rolf, N. Spelten, A. Afchine, D. Fahey, E. Jensen, S. Khaykin, T. Kuhn, P. Lawson, A. Lykov, L. L. Pan, M. Riese, A. Rollins, F. Stroh, T. Thornberry, V. Wolf, S. Woods, P. Spichtinger, J. Quaas, O. Sourdeval, A microphysics guide to cirrus—Part 2: Climatologies of clouds and humidity from observations. *Atmos. Chem. Phys.* **20**, 12569–12608 (2020).
93. K. D. Froyd, P. Yu, G. P. Schill, C. A. Brock, A. Kupc, C. J. Williamson, E. J. Jensen, E. Ray, K. H. Rosenlof, H. Bian, A. S. Darmenov, P. R. Colarco, G. S. Diskin, T. Bui, D. M. Murphy, Dominant role of mineral dust in cirrus cloud formation revealed by global-scale measurements. *Nat. Geosci.* **15**, 177–183 (2022).
94. M. K. Sporre, J. Friberg, C. Svenhag, O. Sourdeval, T. Storelvmo, Springtime stratospheric volcanic aerosol impact on midlatitude cirrus clouds. *Geophys. Res. Lett.* **49**, e2021GL096171 (2022).
95. R. Ullrich, C. Hoose, O. Möhler, M. Niemand, R. Wagner, K. Höhler, N. Hiranuma, H. Saathoff, T. Leisner, A new ice nucleation active site parameterization for desert dust and soot. *J. Atmos. Sci.* **74**, 699–717 (2017).

Acknowledgments: The AERIS/ICARE Data and Services Center provides access to the DARDAR-Nice data. The CloudSat Data Processing Center provides access to the CloudSat data products (http://www.cloudsat.cira.colostate.edu). The data storage and processing are performed on high-performance computers Cheyenne, Casper, and Derecho (doi:10.5065/D6RX99HX) at the NCAR–Wyoming Supercomputing Center provided by the National Science Foundation and the state of Wyoming and supported by NCAR's Computational and Information Systems Laboratory. We would like to thank J. Tackett of NASA Langley for helpful discussion in interpreting the CALIPSO aerosol subtyping product, J. Zhang of Institute of Atmospheric Physics, Chinese Academy of Sciences for providing analysis of the NCEP and ERA5 reanalysis datasets, K. Yang of University of Colorado Boulder for providing analysis of the MLS and AIRS satellite datasets, and X. Shi of Nanjing University of Information Science and Technology for providing the microphysical ice nucleation model with homogeneous freezing. Argonne National Laboratory is operated for the DOE by UChicago Argonne LLC, under contract DE-AC02-06CH11357. Lawrence Livermore National Laboratory is operated by Lawrence Livermore National Security LLC, for the US Department of Energy, National Nuclear Security Administration under contract DE-AC52-07NA27344. **Funding:** This work was supported by Sandia National Laboratories Laboratory Directed Research and Development program (L.L. and X.L.) under contract DE-NA-0003525, Office of Biological and Environmental Research of the US Department of Energy Atmospheric System Research Program THREAD project grant SCW1800 (L.L.), Office of Biological and Environmental Research of the US Department of Energy Energy Exascale Earth System Model (E3SM) project (Y.S.), and National Aeronautics and Space Administration grant 80NSSC19K0341 (K.P.B.). **Author contributions:** Conceptualization: L.L., X.L., Z.K., and X.Z. Methodology: L.L., X.L., K.P.B., Y.S., and X.Z. Investigation: L.L., X.L., Y.S., and X.Z. Visualization: L.L. and X.L. Supervision: X.L. and X.Z. Project administration: X.L. and X.Z. Writing—original draft: L.L. and Y.S. Writing—review and editing: L.L., X.L., Y.S., and X.Z. Resources: L.L., X.L., and X.Z. Data curation: L.L., Y.S., and X.Z. Validation: L.L., Y.S., K.L., and X.Z. Formal analysis: L.L., Y.S., K.L., and X.Z. Software: L.L., K.P.B., K.L., and X.Z. Funding acquisition: X.L. **Competing interests:** The authors declare that they have no competing interests. **Data and materials availability:** All data needed to evaluate the conclusions in the paper are present in the paper and/or the Supplementary Materials. CALIPSO lidar level 3 stratospheric aerosol profile product version 1.00 (DOI: 10.5067/CALIOP/CALIPSO/LID_L3_STRATOSPHERIC_APRO-STANDARD-V1-00) is available from the Atmospheric Science Data Center at NASA LaRC (Fig. 1). CALIPSO lidar level 2 VFM data product version 4-20 (DOI: 10.5067/CALIOP/CALIPSO/LID_L2_VFM-STANDARD-V4-20) is available from the Atmospheric Science Data Center at NASA LaRC (Fig. 2). DARDAR-Nice data are available from the ICARE Data and Services Center (https://www.icare.univ-lille.fr) (Fig. 3). The Cloudsat-CALIPSO 2C-ICE ice cloud microphysics data are available from the CloudSat Data Processing Center run by the Cooperative Institute for Research in the Atmosphere (CIRA) at Colorado State University (https://www.cloudsat.cira.colostate.edu/) (Fig. 3). ERA5 data are available from the Copernicus Climate Data Store (https://cds.climate.copernicus.eu). NCEP FNL data are available from the Research Data Archive at the National Center for Atmospheric Research, Computational and Information Systems Laboratory (https://doi.org/10.5065/D6M043C6). EOS MLS data can be download from https://mls.jpl.nasa.gov/.

Submitted 27 July 2024
Accepted 4 April 2025
Published 9 May 2025
10.1126/sciadv.ads0572

Science Advances

Ice nucleation by volcanic ash greatly alters cirrus cloud properties

Lin Lin, Xiaohong Liu, Xi Zhao, Yunpeng Shan, Ziming Ke, Kai Lyu, and Kenneth P. Bowman

Sci. Adv. **11** (19), eads0572. DOI: 10.1126/sciadv.ads0572

Science Advances (ISSN 2375-2548) is published by the American Association for the Advancement of Science. 1200 New York Avenue NW, Washington, DC 20005. The title *Science Advances* is a registered trademark of AAAS.